Advances in Water Resources 32 (2009) 1664–1673

Contents lists available at ScienceDirect

Advances in Water Resources

journal homepage: www.elsevier.com/locate/advwatres

On breakdown of macroscopic models of mixing-controlled heterogeneous reactions in porous media

I. Battiato [a,1], D.M. Tartakovsky [a,*,1], A.M. Tartakovsky [b,1,2], T. Scheibe [b,1,2]

[a] Department of Mechanical and Aerospace Engineering, University of California, San Diego, La Jolla, CA 92093, USA
[b] Pacific Northwest National Laboratory, P.O. Box 999, Richland, WA 99352, USA

ARTICLE INFO

Article history:
Received 21 May 2009
Received in revised form 26 August 2009
Accepted 26 August 2009
Available online 3 September 2009

Keywords:
Upscaling
Homogeneous reaction
Heterogeneous reaction
Reactive transport
Dissolution
Precipitation

ABSTRACT

Reactive transport in porous media is a complex nonlinear phenomenon that involves both homogeneous (bio-)chemical reactions between species dissolved in a fluid and heterogeneous reactions occurring on liquid–solid interfaces. We establish sufficient conditions under which macroscopic reaction–diffusion equations (RDEs) provide an adequate averaged description of pore-scale processes. These conditions are represented by a phase diagram in a two-dimensional space, which is spanned by Damköhler number and a scale-separation parameter. This phase diagram shows that highly localized phenomena in porous media, including precipitation on (and/or dissolution of) a porous matrix, do not lend themselves to macroscopic (upscaled) descriptions. To compute the predictive errors resulting from the use of macroscopic RDEs, we upscaled the pore-scale RDEs to the continuum (macroscopic) scale and used pore-scale numerical simulations to verify various upscaling assumptions.

1. Introduction

Flow and transport in porous media can be described by employing either pore-scale or Darcy-scale (macroscopic) models. Pore-scale simulations have a solid physical foundation (e.g., Stokes equations for fluid flow and Fick's law of diffusion for solute transport), but require the knowledge of pore geometry that is seldom available. The heterogeneity of most natural porous media and prohibitive computational costs render lattice-Boltzmann modeling, smoothed particle hydrodynamics, and other pore-scale simulations impractical as a predictive tool at scales that are orders of magnitude larger than the pore scale.

Macroscopic models, which treat a porous medium as an "averaged" continuum, overcome these limitations at the cost of relying on phenomenological descriptions, e.g., Darcy's law for fluid flow and an advection–dispersion equation (ADE) for transport. While useful in a variety of applications, such models fail to capture experimentally observed transport features, including a difference between fractal dimensions of the diffusion and dispersion fronts (isoconcentration contours) [14], long tails in breakthrough curves [15], and the onset of instability in variable density flows [28]. ADE-based models of transport of (bio-)chemically reactive solutes, which are the focus of our analysis, can significantly over-predict the extent of reactions in mixing-induced chemical transformations [11, and references therein].

These and other shortcomings stem from the inadequacy of either standard macroscopic models or their parametrizations or both. Upscaling from the pore-scale, on which governing equations are physically based and well defined, to the continuum scale, on which they are used for qualitative predictions, often enables one to establish the connection between the two modeling scales. Mathematical approaches to upscaling include the method of volume averaging [32] and its modifications [9], generalizations of the method of moments [22–24], homogenization via multiple-scale expansions [2], pore-network models [1], and thermodynamically constrained averaging [6]. A number of other approaches to upscaling are reviewed in [4].

Most of these analyses, see also [33,34], deal with physical phenomena described by linear partial differential equations, e.g., dispersion of conservative solutes or solutes undergoing first-order chemical reactions. Nonlinearity of governing equations complicates the upscaling of most reactive transport phenomena. It requires a linearization and/or other approximations, whose accuracy and validity cannot be ascertained a priori. This is especially so for a large class of transport processes, such as mixing-induced precipitation, which exhibit highly localized reacting fronts and consequently defy macroscopic descriptions that are completely decoupled from their microscopic counterparts [17,3,9].

* Corresponding author. Tel.: +1 858 534 1375; fax: +1 858 534 7599.
E-mail address: dmt@ucsd.edu (D.M. Tartakovsky).

[1] This research was supported by the Office of Science of the US Department of Energy (DOE) under the Scientific Discovery through Advanced Computing (SciDAC).
[2] Partial support of this research was provided by project PL-MDT-PD05 funded by the Department of Energy National Nuclear Security Administration at PNNL. The Pacific Northwest National Laboratory is operated for the US Department of Energy by Battelle under Contract DE-AC06-76RL01830.

0309-1708/$ - see front matter © 2009 Elsevier Ltd. All rights reserved.
doi:10.1016/j.advwatres.2009.08.008

Pore-scale simulations of such processes are impractical due to both high computational costs and the lack of detailed information about the pore geometry of porous media larger than a small core. Instead, the localized nature of reaction fronts calls for hybrid simulations [13,29], which resolve a small reactive region with a pore-scale model that is coupled to its continuum counterpart in the rest of a computational domain. (It is worthwhile pointing out that hybrid simulations are not applicable to transport phenomena for which continuum models fail globally rather than locally either because "the connectivity of the pore space or a fluid phase plays a major role" or because of "long-range correlations in the system" [21, p. 1396].)

In this study, we use the method of volume averaging [32] to delineate computational sub-domains where the breakdown of standard continuum models occurs and, hence, a pore-scale component of hybrid simulations is to be employed. Specifically, the method of volume averaging is employed to identify transport regimes for which the assumptions required for the validity of upscaled (macroscopic) equations do not hold, and pore-scale simulations are used to validate this theoretical analysis. To focus on the relative effects of nonlinear geochemical reactions and diffusion, we neglect advection. In the follow up studies, we will consider the effects of advection and employ upscaling approaches other than the method of volume averaging.

In Section 2, we formulate a pore-scale model of mixing-induced precipitation in porous media, which consists of a system of coupled reaction–diffusion equations (RDEs); specify key physical and (bio-)chemical assumptions that underpin this model; and identify Damköhler numbers for homogeneous and heterogeneous reaction as dimensionless parameters that control the phenomenon. In Section 3, we use the local volume averaging [32] to derive a system of upscaled RDEs that are commonly used to model mixing-induced precipitation on the continuum scale, e.g., [25, and the references therein]. The goal here is to identify sufficient conditions for the macroscopic RDEs to be a valid descriptor of mixing-induced precipitation. Section 4 presents the results of pore-scale simulations of mixing-induced precipitation, which unambiguously show that these conditions are not met.

2. Pore-scale description of mixing-controlled heterogeneous reactions

Consider a porous medium Ω that is fully saturated with an incompressible liquid at rest. The medium consists of a solid matrix Ω_s and a liquid-occupied pore space Ω_l, so that $\Omega = \Omega_s \cup \Omega_l$. The liquid is a solution of two chemical (or biological) species M_1 and M_2 (with respective concentrations c_1^* and c_2^*) that react to form an aqueous reaction product M_3. Whenever c_3^*, the concentration of M_3, exceeds a threshold value, M_3 undergoes a heterogeneous reaction and precipitates on the solid matrix, forming a precipitate $M_{4(s)}$. In general, this process of mixing-induced precipitation is fully reversible, $M_1 + M_2 \rightleftarrows M_3 \rightleftarrows M_{4(s)}$, and its speed is controlled by the reaction rates k_{12} ($\mathrm{L^3\,mol^{-1}\,T^{-1}}$), k_p ($\mathrm{L\,T^{-1}}$), k_3 ($\mathrm{T^{-1}}$), and k_d ($\mathrm{mol\,T^{-1}\,L^{-2}}$) corresponding to the following reactions,

$$M_1 + M_2 \overset{k_{12}}{\rightarrow} M_3 \overset{k_p}{\rightarrow} M_{4(s)} \quad \text{and} \quad M_1 + M_2 \overset{k_3}{\leftarrow} M_3 \overset{k_d}{\leftarrow} M_{4(s)}. \tag{1}$$

For bimolecular and unimolecular elementary reactions at constant temperature, the change in concentration is proportional to the product of the concentrations of the reactants. Hence, the consumption and production rates, R_i^c with $i \in \{1,2\}$ and R_3^p, of species $M_i, i \in \{1,2\}$, and M_3, respectively, associated with the homogeneous reaction in (1) are typically concentration-driven and of the form $R_i^c = -R_3^p = -k_{12}c_1^*c_2^* + k_3c_3^*$. For the heterogeneous reaction, it is common to assume [10,5, and references therein] that (i) precipitation rate r_p is proportional to concentration c_3^*, i.e., $r_p = k_pc_3^*$; (ii) dissolution rate r_d is constant, $r_d = k_d$; and (iii) the super-saturation index does not become large enough to support precipitation in the liquid phase, i.e., precipitation of M_3 occurs solely as an overgrowth on solid grains.

With these assumptions, the aqueous concentrations $c_i^*(\mathbf{r}^*, t^*)$ ($\mathrm{mol\,L^{-3}}$) at point $\mathbf{r}^*$ and time t^* satisfy a system of reaction–diffusion equations (RDEs),

$$\frac{\partial c_i^*}{\partial t^*} = \mathscr{D}_i\nabla_*^2c_i^* - k_{12}c_1^*c_2^* + k_3c_3^* \quad \text{for } \mathbf{r}^* \in \Omega_l,\ t^* > 0, \quad i = 1,2, \tag{2a}$$

$$\frac{\partial c_3^*}{\partial t^*} = \mathscr{D}_3\nabla_*^2c_3^* + k_{12}c_1^*c_2^* - k_3c_3^* \quad \text{for } \mathbf{r}^* \in \Omega_l,\ t^* > 0 \tag{2b}$$

subject to the boundary conditions on the (multi-connected) liquid–solid interface $\mathscr{A}_{ls}$

$$\mathbf{n}\cdot\nabla_*c_i^* = 0,\ \ i = 1,2; \quad -\mathscr{D}_3\mathbf{n}\cdot\nabla_*c_3^* = k_p\left(c_3^* - c_{\mathrm{eq}}\right) \tag{3}$$

and the initial conditions

$$c_i^*(\mathbf{x},0) = c_{i0}(\mathbf{x}),\ \ i = 1,2,3, \quad \Omega_l(0) = \Omega_{l0}, \tag{4}$$

when concentration of $M_{4(s)}$ is strictly positive. Here the starred (*) quantities have appropriate units (physical dimensions), $c_{\mathrm{eq}} = k_d/k_p$ is the equilibrium concentration, $\mathscr{D}_i$ ($\mathrm{L^2\,T^{-1}}$) ($i = 1,2,3$) are the diffusion coefficients of the aqueous species M_1, M_2, and M_3, respectively. Due to precipitation and dissolution, the liquid–solid interface $\mathscr{A}_{ls}(t^*)$, with the outward normal unit vector $\mathbf{n}(t^*)$, evolves in time t^* with velocity $\mathbf{v}$ ($\mathrm{L\,T^{-1}}$), according to $\rho_c\mathbf{v}\cdot\mathbf{n} = k_p(c_3^* - c_{\mathrm{eq}})$, where ρ_c ($\mathrm{mol_s\,L^{-3}}$) is the molar density of the precipitate. The dynamics of the interface $\mathscr{A}_{ls}(t^*)$ result from a modeling assumption about the dependence of $\mathbf{v}$ on precipitation/dissolution rates and mass conservation [30].

Under certain assumptions, the system of RDEs (2) can be simplified by neglecting intermediate reactions [8,25,27, and the references therein]. In particular, if in (2b) reactions are faster than diffusion, and the diffusive term dominates the time-evolution term, then (2b) yields $c_3 \approx k_{12}/k_3c_1c_2$. Under these assumptions, the system (2)–(3) reduces to a system of two equations for c_i^* ($i = 1,2$): $\partial c_i^*/\partial t^* = \mathscr{D}_i\nabla_*^2c_i^*$ subject to the interfacial conditions $\mathbf{n}\cdot\nabla_*c_i^* = 0$ and $\rho_c\mathbf{v}\cdot\mathbf{n} = k_c(c_1^*c_2^*/k_{sp} - 1)$, where $k_c = k_pc_{\mathrm{eq}}$ and $k_{sp} = k_3c_{\mathrm{eq}}/k_{12}$ is the solubility product. Calcite precipitation from calcium bicarbonate in water saturated with carbon dioxide, which follows the reaction path $Ca^{2+} + 2HCO_3^- \leftrightarrow Ca(HCO_3)_{2(l)} \leftrightarrow CaCO_{3(s)} + CO_{2(g)} + H_2O$, provides an example of geochemical systems for which these assumptions are not valid [20,7]. For the sake of generality, we consider a more comprehensive system (2).

To be specific, we consider a scenario in which two identical solvents (e.g., water), one containing M_1 with concentration c_{10}^* and the other containing M_2 with concentration c_{20}^*, are brought in contact with each other at time $t^* = 0$. Since reactants M_1 and M_2 are initially separated, no reactions took place and the initial concentration of reaction product M_3 is $c_{30}^* = 0$. This is a typical situation, corresponding, for example, to injection of a solution of M_1 into a porous medium occupied by a solution of M_2 [27].

The characteristic time scales associated with the chemical reactions (1) are $\tau_1 = \tau_2 = 1/k_{12}c_{10}$ for concentrations c_1^* and c_2^*, and $\tau_3 = c_{\mathrm{eq}}/k_{12}c_{10}^2$ for concentration c_3^*. To simplify the presentation, we assume that the diffusion coefficients for reactants M_1 and M_2 and product M_3 are the same, $\mathscr{D}_1 = \mathscr{D}_2 = \mathscr{D}_3 = \mathscr{D}$. Let us introduce dimensionless quantities

$$t = \frac{t^*}{\tau}, \quad q = \frac{c_{\mathrm{eq}}}{c_{10}}, \quad c_i = \frac{c_i^*}{c_{10}}, \quad c_3 = \frac{c_3^*}{c_{\mathrm{eq}}}, \quad K = \frac{k_3c_{eq}}{k_{12}c_{10}^2},$$

$$Da = \frac{l_l^2k_{12}c_{10}}{\mathscr{D}}, \tag{5}$$

where $i = 1,2; l_l$ denotes a characteristic length scale associated with pore-structure; and Damköhler number Da is the ratio of diffusion and reaction time scales for species M_i ($i = 1,2,3$). RDEs (2) can now be written in a dimensionless form as

$$\frac{\partial c_i}{\partial t} = \frac{l_l^2}{Da}\nabla_*^2 c_i - c_1 c_2 + K c_3 \quad (i = 1,2),$$
$$q\frac{\partial c_3}{\partial t} = \frac{q l_l^2}{Da}\nabla_*^2 c_3 + c_1 c_2 - K c_3. \tag{6}$$

Following [26], we define a Damköhler number for the precipitation/dissolution process as

$$Da_{ls} = \frac{k_p l_l}{\mathscr{D}}. \tag{7}$$

This yields a dimensionless form of the boundary conditions on the liquid–solid interface $\mathscr{A}_{ls}$,

$$\mathbf{n}\cdot\nabla_* c_i = 0 \quad (i = 1,2), \quad \mathbf{n}\cdot l_l \nabla_* c_3 = Da_{ls}(1 - c_3). \tag{8}$$

3. Macroscopic description of mixing-controlled heterogeneous reactions

We proceed by employing the local volume averaging [32] to upscale the pore-scale equations (6) and (8) to the macroscopic scale. Section 3.1 contains definitions of the averaging procedure. The derivation of upscaled equations is presented in Section 3.2. The results are summarized in Section 3.3, which presents a phase diagram identifying sufficient conditions under which the upscaled (macroscopic) description is valid.

3.1. Preliminaries

Consider a volume of the porous medium $\mathscr{V} \in \Omega$ whose size is $|\mathscr{V}|$ and characteristic radius $r_0 \gg l_l$, where l_l is the pore-geometry length scale. Let $V_l(\mathbf{x}^*) \in \mathscr{V}$ denote the liquid phase contained in $\mathscr{V}$, which is centered at $\mathbf{x}^* \in \Omega$. If a characteristic length-scale of the macroscopic domain Ω is L, then the size of the averaging volume $\mathscr{V}$ is selected to satisfy $l_l \ll r_0 \ll L$.

Following [32], we define *superficial* and *intrinsic* averages of a quantity $c(\mathbf{r}^*)$ with $\mathbf{r}^* \in V_l$ as

$$\langle c\rangle(\mathbf{x}^*) = \frac{1}{|\mathscr{V}|}\int_{V_l(\mathbf{x}^*)} c(\mathbf{r}^*)\mathrm{d}^3 r \quad \text{and}$$
$$\langle c\rangle^l(\mathbf{x}^*) = \frac{1}{|V_l(\mathbf{x}^*)|}\int_{V_l(\mathbf{x}^*)} c(\mathbf{r}^*)\mathrm{d}^3 r, \tag{9}$$

respectively. The two averages are related through porosity $\phi \equiv |V_l|/|\mathscr{V}|$ by $\langle c\rangle = \phi\langle c\rangle^l$. The application of spatial averaging is facilitated by the spatial averaging theorem [32],

$$\langle\nabla_* c\rangle = \nabla_*\langle c\rangle + \frac{1}{|\mathscr{V}|}\int_{A_{ls}} c\mathbf{n}\,\mathrm{d}A, \tag{10}$$

where $A_{ls}(\mathbf{x}^*) = \mathscr{V}\cap V_l(\mathbf{x}^*)$ is the liquid–solid interface contained in $\mathscr{V}$.

Let L_c, L_{c1}, and L_ϕ denote characteristic length-scales associated with the macroscopic quantities $\langle c\rangle^l, \nabla_*\langle c\rangle^l$ and ϕ, respectively. These scales are defined by [32, p. 19]

$$\nabla_* f_i(x) = \mathscr{O}\left(\frac{\Delta f_i}{L_i}\right), \quad \Delta f_i(x) \equiv f_i\left(x + \frac{L_i}{2}\right) - f_i\left(x - \frac{L_i}{2}\right) \tag{11}$$

for $f_i = \{\langle c\rangle^l, \nabla_*\langle c\rangle^l, \phi\}$ and $L_i = \{L_c, L_{c1}, L_\phi\}$, respectively. The notation

$$f = \mathscr{O}(g) \tag{12}$$

denotes an order of magnitude estimate in the following sense [12, p. 391]:

$$\frac{|g|}{\sqrt{10}} \leqslant |f| \leqslant |g|\sqrt{10}. \tag{13}$$

3.2. Upscaling via volume averaging

In this section, we upscale the third equation in (6). The remaining two equations in (6) are upscaled in a similar fashion.

We assume that reactions in the fluid phase are much faster than precipitation on the solid phase, so that $\langle\partial c_3/\partial t\rangle = \partial\langle c_3\rangle/\partial t$. No assumptions are required for the upscaling of the linear term $\langle Kc_3\rangle^l = K\langle c_3\rangle^l$. The averaging procedure is presented below as a series of propositions. Their proofs are provided in the Appendix A.

Proposition 3.1. *Suppose that the following scale constraints hold:*

1) $l_l \ll r_0$,
2) $r_0^2 \ll \bar{L}^2$ *where* $\bar{L} = min\{L_{c1}, L_\phi\}$,
3) $\epsilon \ll 1$ *where* $\epsilon = l_l/L_c$,
4) $r_0 \ll L_c$,
5) $r_0^2 \ll L_c L_{c1}$.

Then the average of the Laplacian in (6) can be approximated by

$$\langle\nabla_*^2 c_3\rangle = \phi\nabla_*^2\langle c_3\rangle^l + \nabla_*\phi\cdot\nabla_*\langle c_3\rangle^l + \frac{1}{|\mathscr{V}|}\nabla_*\cdot\int_{A_{ls}}\tilde{c}_3\mathbf{n}_{ls}\,\mathrm{d}A - a_v Da_{ls}\frac{\langle c_3\rangle^l - 1}{l_l}, \tag{14}$$

where $a_v \equiv |\mathscr{A}_{ls}|/|\mathscr{V}|$ *and* $\tilde{c}_3$ *is such that* $c_3 = \langle c_3\rangle^l + \tilde{c}_3$.

The scale constraints of Proposition 3.1 are routinely used in the method of volume averaging and other upscaling techniques to define the size of the averaging volume $\mathscr{V}$, which might or might not constitute a representative elementary volume (REV). Constraints 1 and 4 require $\mathscr{V}$ to be large enough to smooth out (average) pore-scale fluctuations of relevant variables (e.g., concentration) and small enough to capture their macro-scale variability, respectively. The remaining constraints guarantee that the average concentration at the centroid of $\mathscr{V}$ provides an adequate representation of the pore-scale concentration distribution at all points inside $\mathscr{V}$ [32].

Proposition 3.2. *Suppose that the scale constraints 3)–5) of the Proposition 3.1 hold. Then the average of the reaction term in (6) can be approximated by*

$$\langle c_1 c_2\rangle = \phi\langle c_1\rangle^l\langle c_2\rangle^l. \tag{15}$$

While the approximation (15) can be improved upon, its importance for the present analysis stems from the observation that it does not introduce additional scale constraints.

Proposition 3.3. *Suppose that in addition to the constraints in Proposition 3.1 the following scale constraints hold:*

1) $a_v \approx l_l^{-1}$,
2) $t \gg Da$,
3) $l_l \ll L_\phi$.

Then, the concentration fluctuations $\tilde{c}_3$ *satisfy a differential equation*

$$0 = \frac{q l_l^2}{Da}\nabla_*^2\tilde{c}_3 + \frac{q a_v l_l}{\phi}\frac{Da_{ls}}{Da}(\langle c_3\rangle^l - 1) + \tilde{c}_1\langle c_2\rangle^l + \tilde{c}_2\langle c_1\rangle^l + \tilde{c}_1\tilde{c}_2 - K\tilde{c}_3 \tag{16}$$

subject to the boundary conditions

$$-\mathbf{n}\cdot\nabla_*\tilde{c}_3 = \mathbf{n}\cdot\nabla_*\langle c_3\rangle^l + Da_{ls}\frac{\langle c_3\rangle^l + \tilde{c}_3 - 1}{l_l}. \tag{17}$$

The scale constraint 1) corresponds to representations of solid grains by spheres, in which case specific surface a_v, surface A_{ls}, and volume V_l scale as l^{-1}, l^2, and l^3, respectively. The constraint 3) ensures that porosity changes smoothly enough for its gradient to be negligible.

Boundary-value problems for fluctuations $\tilde{c}_1$ and $\tilde{c}_2$ are derived in a similar manner. Further progress requires an assumption of periodicity of the porous medium.

Proposition 3.4. *Suppose that in addition to the scale constraints imposed by Propositions 3.1 and 3.3 the porous medium is periodic with a unit cell characterized by* $\mathbf{n}(\mathbf{r}^* + \mathbf{l}_i^*) = \mathbf{n}(\mathbf{r}^*)$, *where* $\mathbf{l}_i^*$ *with* $i = 1,2,3$ *represents the three lattice vectors describing a spatially periodic porous medium. Then concentration fluctuations are periodic,* $\tilde{c}(\mathbf{r}^* + \mathbf{l}_i^*) = \tilde{c}(\mathbf{r}^*)$, *and* $\langle c_3\rangle^l$ *and* $\nabla_*\langle c_3\rangle^l$ *in (16) and (17) are evaluated at the centroid.*

Mathematical representations of natural porous media as a periodic collection of unit cells might appear to be overly restrictive. However, this assumption often leads to homogenization results (effective or continuum models) that are applicable to more realistic heterogeneous environments. A detailed discussion of the practical utility of periodic conceptualizations of the pore-structure of porous media can be found in Section 2 of [16].

Proposition 3.5. *Suppose that in addition to the constraint imposed by Proposition 3.3 the following constraints hold:*

1) $Da_{ls} \ll \epsilon$,
2) $Da \ll 1$.

Then concentration fluctuations $\tilde{c}_3$ *can be represented in terms of the macroscopic variables as*

$$\tilde{c}_3 = \mathbf{b}^* \cdot \nabla_*\langle c_3\rangle^l + s\langle c_3\rangle^l + \psi, \tag{18}$$

where the closure variables $\mathbf{b}^*, s$ *and* ψ *are solutions of the boundary-value problems (wherein* $j = 1,2,3$*)*

$$\nabla_*^2\mathbf{b}^* - \frac{k_3}{\mathscr{D}}\mathbf{b}^* = \mathbf{0}, \quad -\mathbf{n}\cdot\nabla_*\mathbf{b}^* = \mathbf{n} \text{ at } A_{ls}, \quad \mathbf{b}^*(\mathbf{r}^* + \mathbf{l}_j^*) = \mathbf{b}^*(\mathbf{r}^*); \tag{19}$$

$$\nabla_*^2 s - \frac{k_3}{\mathscr{D}}s = -\frac{a_v Da_{ls}}{\phi l_l},$$
$$-\mathbf{n}\cdot\nabla_* s = \frac{Da_{ls}}{l_l}\langle c_3\rangle^l \text{ at } A_{ls}, \quad s\left(\mathbf{r}^* + \mathbf{l}_j^*\right) = s(\mathbf{r}^*); \tag{20}$$

$$\nabla_*^2\psi - \frac{k_3}{\mathscr{D}}\psi = \frac{a_v Da_{ls}}{\phi l_l},$$
$$-\mathbf{n}\cdot\nabla_*\psi = -\frac{Da_{ls}}{l_l} \text{ at } A_{ls}, \quad \psi\left(\mathbf{r}^* + \mathbf{l}_j^*\right) = \psi(\mathbf{r}^*). \tag{21}$$

The conditions 1) and 2) ensure that the system is well-mixed at the pore scale, as discussed in Section 3.3.

Combining the results from Propositions 3.1–3.5 with analogous results for $\langle c_1\rangle^l$ and $\langle c_2\rangle^l$, the volume averaging of (6) leads to a system of macroscopic equations (see Appendix A.6)

$$\phi\frac{\partial\langle c_i\rangle^l}{\partial t} = \frac{\epsilon^2}{Da}\nabla\cdot(\phi\mathbf{D}_{\text{eff}}\cdot\nabla\langle c_i\rangle^l) - \phi\langle c_1\rangle^l\langle c_2\rangle^l + \phi K\langle c_3\rangle^l \quad (i = 1,2), \tag{22}$$

$$\phi q\frac{\partial\langle c_3\rangle^l}{\partial t} = \frac{q\epsilon^2}{Da}\nabla\cdot(\phi\mathbf{D}_{\text{eff}}\cdot\nabla\langle c_3\rangle^l) - qa_v l_l\frac{Da_{ls}}{Da}[\langle c_3\rangle^l - 1] + \phi\langle c_1\rangle^l\langle c_2\rangle^l - \phi K\langle c_3\rangle^l, \tag{23}$$

where the effective diffusivity tensor $\mathbf{D}_{\text{eff}}$ is defined as

$$\mathbf{D}_{\text{eff}} = \mathbf{I} + \frac{1}{|V_l|}\int_{A_{ls}}\mathbf{n}\mathbf{b}^*\,dA. \tag{24}$$

3.3. Applicability of macroscopic models

According to Proposition 3.5, a sufficient condition for the validity of the macroscopic description (22) and (23) requires that $Da \ll 1$, which implies that on the pore scale the system is well-mixed with diffusion dominating reactions. Further insight is gained by relating different macroscopic diffusion and/or reaction regimes to the Damköhler number Da expressed in terms of the scale-separation parameter ϵ. (This is conceptually similar to the analysis of macroscopic dispersion equations [3], which identifies distinct transport regimes by expressing the Péclet number as powers of ϵ.) Interplay between the Damköhler number and ϵ determines whether macroscopic RDEs (22) and (23) are diffusion or reaction dominated. For $Da < \epsilon^2$, the macroscopic process is diffusion-driven and the nonlinear effects introduced by reactions are negligible. The two mechanisms are of the same order of magnitude in the region $\epsilon^2 < Da < \epsilon$, while reactions dominate diffusion if $\epsilon < Da < 1$.

Combining constraints 1) and 4) of Proposition 3.1 and 1) of Proposition 3.4, we can write $l_l \ll r_0 \ll \min\{L_c, L_{c1}\}$. As an example, let us assume that $L_c = \min\{L_c, L_{c1}\}$, where L_c is the typical length scale associated with the average concentration, as defined by (11). Recalling the operational definition of the order of magnitude $\mathcal{O}(\cdot)$ in (12) and (13) and the definition of ϵ in Proposition 3.1, we obtain a constraint $\epsilon \leqslant 10^{-3}$.

Fig. 1 summarizes these constraints in the form of a phase diagram. The solid red line, which is composed of the straight lines $Da = 1$, and $\epsilon = 10^{-3}$, separates the region where the macroscopic model (22) and (23) is valid (to the right of the red line) and the region where it is a priori not (to the left of the red line). The dashed blue lines $Da = \epsilon^2$ and $Da = \epsilon$ separate the diffusion-dominated, diffusion–reaction, and reaction-dominated regimes for (22) and (23). In the region $\epsilon^{-1} < Da < 1$, a system of equations

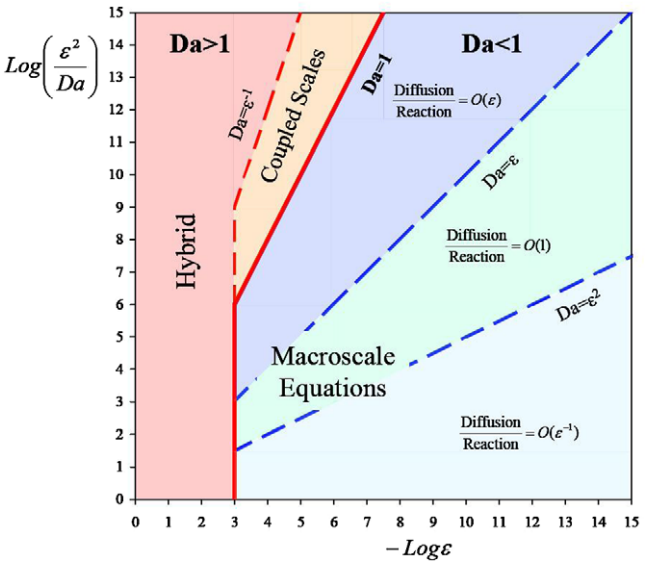

Fig. 1. Phase diagram indicating the range of applicability of macroscopic equations for the reaction–diffusion system (6) in terms of Da. The blue regions identify the sufficient conditions under which the macroscopic equations hold. In the red and orange regions, macro- and micro-scale problems are coupled and have to be solved simultaneously. (For interpretation of the references to colour in this figure legend, the reader is referred to the web version of this article.)

for pore-scale fluctuations [17] must be solved *simultaneously* with a macroscopic problem (see Appendix A.6). This region is labeled "Coupled Scales" in Fig. 1. Mixing-induced precipitation, which is characterized by $Da \gg 1$, falls into the category of physical phenomena for which pore-scale or hybrid simulations are necessary.

4. Comparison with pore-scale simulations

In this section, we use pore-scale numerical simulations of (6) and (8) with $Da > 1$ both to demonstrate that the constraints imposed by the averaging procedure outlined above are indeed not satisfied in the region "Hybrid" of the phase diagram in Fig. 1 and to quantify various approximation errors. A computational example with $Da = 4.4 \cdot 10^{-4}$, which represents the region in Fig. 1 where continuum models are expected to be valid, can be found in [29].

The RDEs (6) are defined for the pore space of a two-dimensional porous medium $[-L/2, L/2] \times [0, B]$, with $L = 32$ and $B = 8$. The porous medium is composed of circular grains with radius $l_l = 3$, which form periodically arranged unit cells, as shown in Fig. 2. In addition to the boundary conditions (8), the RDEs (6) are subject to the exterior boundary conditions $\partial_x c_1(L/2, y, t) = 0$, $\partial_x c_2(-L/2, y, t) = 0$, $\partial_x c_3(\pm L/2, y, t) = 0$, $c_1(-L/2, y, t) = 1$, and $c_2(L/2, y, t) = 1$. The periodic boundary conditions are prescribed at $y = 0$ and $y = B$. The initial conditions are $c_1(-L/2 \leqslant x \leqslant 0, y) = 1$, $c_1(0 < x \leqslant L_2, y) = 0$, $c_2(-L/2 \leqslant x < 0, y) = 1$, and $c_2(0 \leqslant x \leqslant L_2, y) = 0$.

4.1. Numerical implementation

We used the mesh-free Smoothed Particle Hydrodynamics (SPH) simulations [26,29] to solve this initial-boundary-value problem. SPH "particles" were placed on square lattices whose size is $\Delta x = \Delta y = 0.25$. Table 1 presents the parameter values used in these simulations. We consider $K \ll 1$ so that the backward homogeneous reaction can be neglected.

The macroscopic quantities, such as $\langle c_1 \rangle$, were computed from the pore-scale simulations by averaging over a volume $\mathscr{V}$ whose characteristic dimension is $r_0 \gg l_l$. Following [19], we define the size of the averaging volume, i.e., the value of r_0, as the minimum radius of $\mathscr{V}$ beyond which porosity ϕ remains constant as the averaging volume increases. For the geometric parameters used in our simulations, this yields $r_0 = 125$ which clearly satisfies the inequality $r_0 \gg l_l$. The intrinsic average $\langle c_1 \rangle^l$ in (9) was computed as

$$\langle c_1 \rangle^l(\mathbf{x}) \approx \frac{1}{N(\mathbf{x})} \sum_{b \in \mathscr{V}} c_1(\mathbf{y}_b) W_{\mathbf{x}, r_0}(\mathbf{y}_b), \tag{25}$$

where $N(\mathbf{x})$ is the number of liquid SPH "particles" contained in $\mathscr{V}(\mathbf{x})$, $\mathbf{y}_b$ is the position of the "particle" b, and

$$W_{\mathbf{x}, r_0}(\mathbf{y}) = \begin{cases} 1 & \text{if } |\mathbf{y} - \mathbf{x}| \leqslant r_0, \\ 0 & \text{if } |\mathbf{y} - \mathbf{x}| > r_0. \end{cases} \tag{26}$$

Table 1
Parameter values (in model units) and corresponding dimensionless quantities used in pore-scale simulations.

Parameters	Units	Dimensionless parameters
$\mathscr{D} = 0.5$	$\mathrm{L}^2\,\mathrm{T}^{-1}$	$Da = 27$
$k_{12} c_{10} = 1.5$	T^{-1}	$Da_{ls} = 120$
$k_p = 20$	$\mathrm{L}\,\mathrm{T}^{-1}$	$q = 0.3$
$c_{eq} = 0.15$	$\mathrm{mol}\,\mathrm{L}^{-2}$	
$c_{eq}/c_{10} = 0.3$	–	

4.2. Simulation results

We start by investigating whether the mixing-induced precipitation described on the pore scale by the system of RDEs (6) lends itself to scale separation. It follows from (11) and (13) that

$$|\nabla \langle c_1 \rangle^l| \leqslant \frac{|\Delta \langle c_1 \rangle^l|}{L_c} \sqrt{10} \leqslant \frac{\sqrt{10}}{L_c}, \tag{27}$$

where the second inequality stems from the bound $|\Delta \langle c \rangle^l| \leqslant 1$, since $0 \leqslant \langle c \rangle^l \leqslant 1$. Using an operational definition of $\gg$ [31, p. 13], we express the constraint $L_c \gg r_0$, imposed by Proposition 3.1, in terms of an inequality $L_c \geqslant 10 r_0$. Substituting this inequality into (27) gives an upper bound of the gradient of the average concentration,

$$|\nabla \langle c_1 \rangle^l| \leqslant \frac{1}{\sqrt{10} r_0}, \tag{28}$$

which serves as a *necessary condition* for the scale separation to occur.

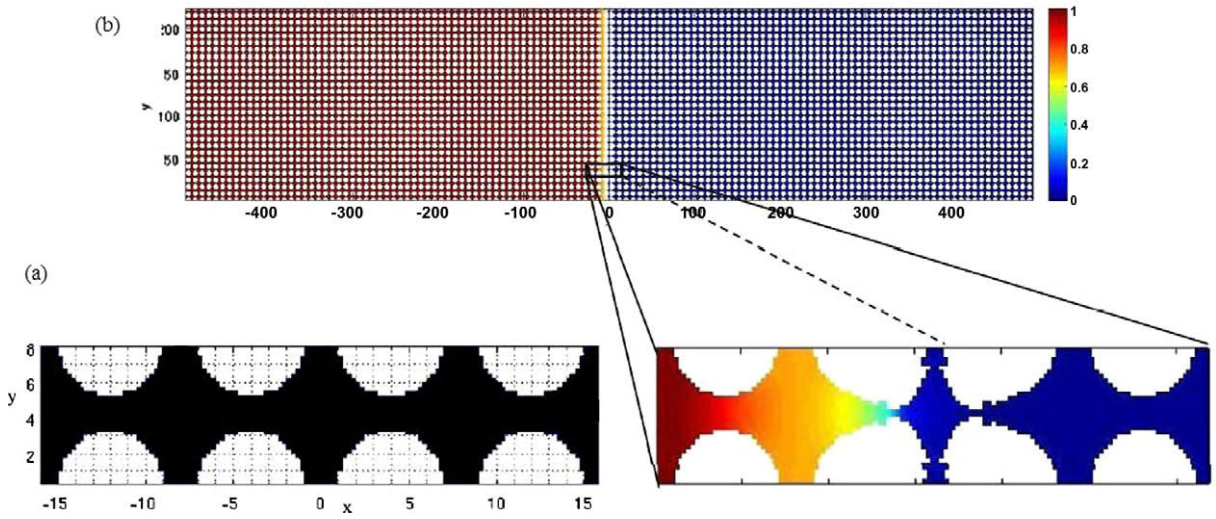

Fig. 2. (a) Schematic representation of a unit cell of the porous medium at the pore scale. White spaces represent solid grains. (b) Concentration distribution for c_1 in the macroscopic domain, obtained by replicating the unit cell in the y-direction.

Fig. 3a exhibits profiles of $c_1(x)$ and $\langle c_1\rangle^l(x)$ along the cross-section $y = B/2 + nB,\ n = \{0, 1, 2\ldots\}$, which lies entirely in the fluid phase. Numerical differentiation was further used to compute $\nabla\langle c_1\rangle^l$ along this cross-section. Small oscillations of the intrinsic average $\langle c_1\rangle^l(x)$ in Fig. 3a stem from its definition (9). As the averaging window of size $|\mathscr{V}|$ moves from left to right, the pore volume V_l varies periodically, giving rise to large periodic oscillation in $\nabla\langle c_1\rangle^l$ (Fig. 3b). One can see that the smoothed (average) gradient is $\nabla\langle c_1\rangle^l \approx \Delta\langle c_1\rangle^l/\Delta x \approx 1/200 = 0.005$, so that the bound (28) is not satisfied in the vicinity of the reacting front. This violates the constraint $L_c \gg r_0$ imposed by Proposition 3.1.

We now proceed to analyze how the lack of scale separation affects the accuracy of the closure approximation $\langle c_1c_2\rangle^l \approx \langle c_1\rangle^l\langle c_2\rangle^l$, on which the macroscopic RDEs (22) and (23) are based. The proof of Proposition 3.2 in Appendix A.2 demonstrates that this closure requires one to neglect the terms $\langle\tilde{c}_1\tilde{c}_2\rangle^l, \langle\tilde{c}_1\langle c_2\rangle^l\rangle^l$ and $\langle\tilde{c}_2\langle c_1\rangle^l\rangle^l$, and to assume that $\langle\langle c_1\rangle^l\langle c_2\rangle^l\rangle^l \approx \langle c_1\rangle^l\langle c_2\rangle^l$. The results of our pore-scale simulations shown in Fig. 4 reveal that both $\langle\langle c_1\rangle^l\langle c_2\rangle^l\rangle^l$ and $\langle c_1\rangle^l\langle c_2\rangle^l$ significantly overestimate $\langle c_1c_2\rangle^l$.

This finding is further elaborated upon in Fig. 5, which depicts the relative errors in progressively improved approximations of the term $\langle c_1c_2\rangle^l$,

$$E_i^{\%} = \frac{|E_i|}{\langle c_1c_2\rangle^l}, \quad i = 1, \ldots, 4, \tag{29}$$

where $E_1 = \langle c_1\rangle^l\langle c_2\rangle^l - \langle c_1c_2\rangle^l, E_2 = E_1 + \langle\tilde{c}_1\tilde{c}_2\rangle^l, E_3 = E_2 + \langle\tilde{c}_1\langle c_2\rangle^l\rangle^l$, and $E_4 = E_3 + \langle\tilde{c}_2\langle c_1\rangle^l\rangle^l$. While the incorporation of more fluctuating terms slightly decreases the relative errors, they remain unacceptably high even when all the terms are included ($E_4^{\%} \approx 10^3$). This shows that $\langle\langle c_1\rangle^l\langle c_2\rangle^l\rangle^l \approx \langle c_1\rangle^l\langle c_2\rangle^l$ is the weakest approximation. (Recall that the definition of the intrinsic average $\langle\cdot\rangle^l$ in (9) implies that this indeed is only an approximation.) This finding is to be expected, since for $L_c = \mathscr{O}(l_l)$ a Taylor expansion around the centroid does not provide an accurate description of nonlocal terms.

5. Conclusions

Reactive transport in fully saturated porous media is a complex nonlinear phenomenon that involves both homogeneous (bio-)chemical reactions between species dissolved in a fluid and heterogeneous reactions that occur on liquid–solid interfaces. We considered processes that are dominated by two transport mechanisms, molecular diffusion and (bio-)chemical reactions, whose relative importance is quantified by the (dimensionless) Damköhler number *Da*. Specifically, we considered mixing-induced precipitation, in which two dissolved reactants produce a third species that, after reaching a threshold concentration value, precipitates on the solid matrix.

Our main goal was to establish sufficient conditions under which macroscopic reaction–diffusion equations (RDEs) provide an adequate averaged description of pore-scale processes, and to quantify predictive errors that occur when some or all of these conditions are violated. To accomplish this goal, we upscaled the pore-scale RDEs to the continuum (macroscopic) scale and used

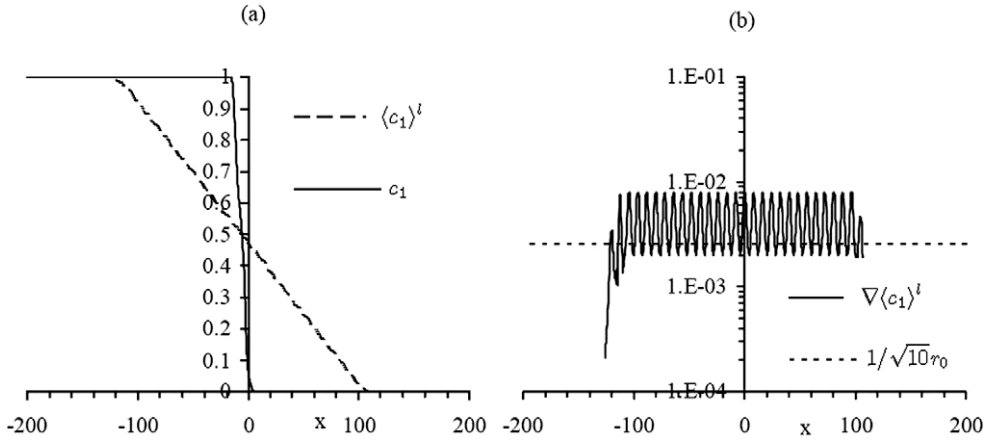

Fig. 3. Horizontal cross-sections at $t = 15,400$ of (a) pore-scale concentration c_1 and its intrinsic average $\langle c_1\rangle^l$, and (b) the horizontal component of the average concentration gradient $\nabla\langle c_1\rangle^l$.

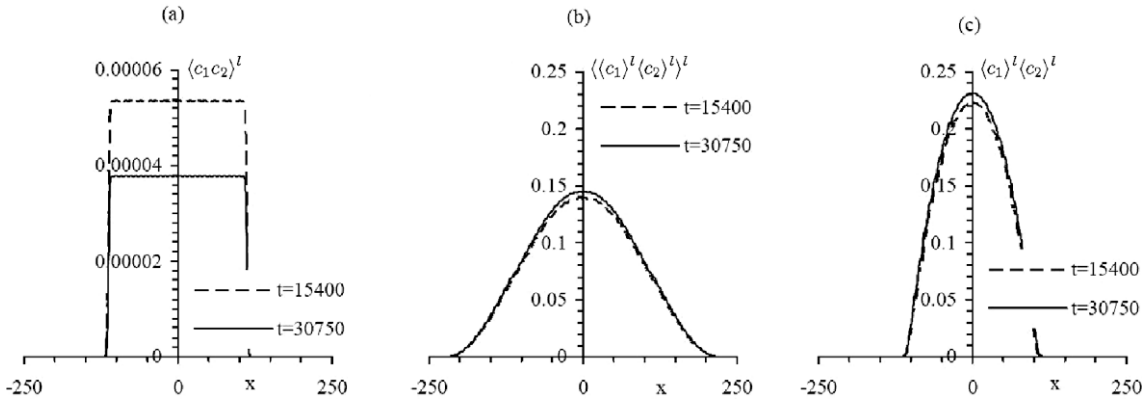

Fig. 4. Horizontal cross-sections of (a) $\langle c_1c_2\rangle^l$ and its approximations, (b) $\langle\langle c_1\rangle^l\langle c_2\rangle^l\rangle^l$ and (c) $\langle c_1\rangle^l\langle c_2\rangle^l$.

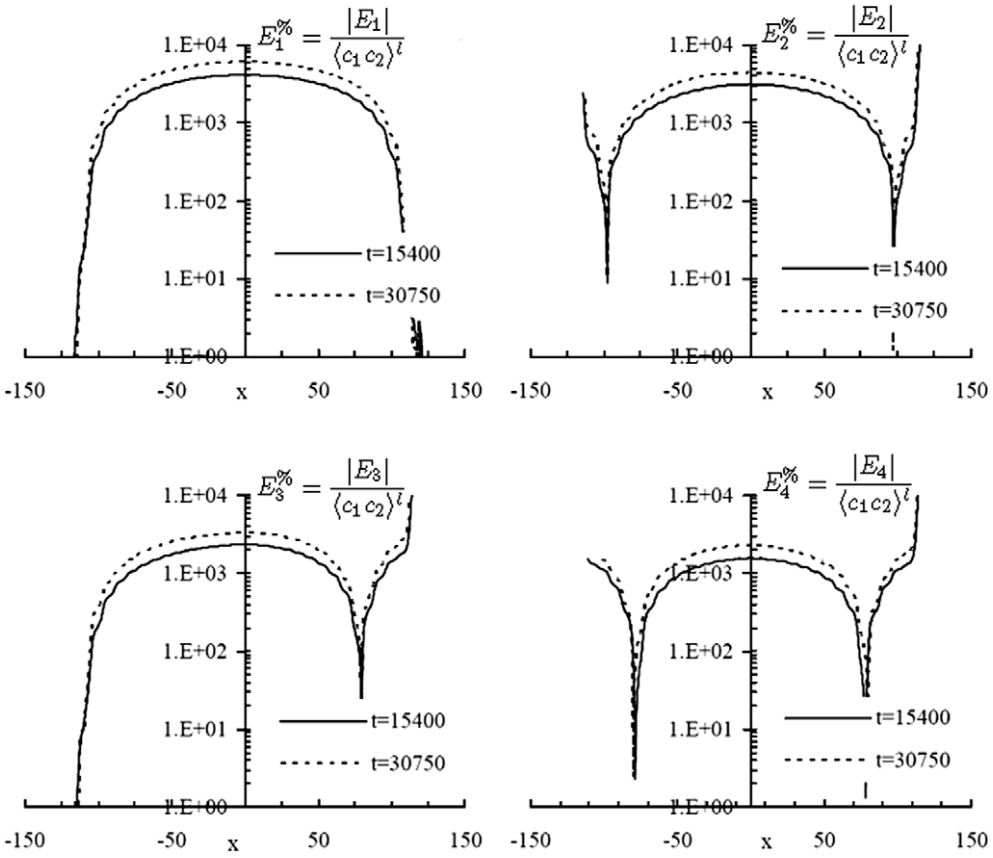

Fig. 5. Relative errors $E_i^{\%}$ $(i = 1, \ldots, 4)$ in (29) introduced by various closure approximations.

pore-scale numerical simulations to verify various upscaling assumptions. Our analysis leads to the following major conclusions.

(1) The range of applicability of macroscopic RDEs and various transport regimes can be described with a phase diagram (Fig. 1) in the (Da, ϵ) space; where Da is the Damköhler number and ϵ is the scale-separation parameter defined as the ratio of the characteristic lengths associated with pore-scale geometry and macroscopic concentrations of reacting species, respectively.
(2) This phase diagram shows that highly localized phenomena in porous media, such as mixing-induced precipitation on (and/or dissolution of) a porous matrix, do not lend themselves to macroscopic (upscaled) descriptions. The use of macroscopic RDEs, such as (22) and (23), to describe such phenomena relies on a number of approximations whose accuracy cannot be ascertain a priori.
(3) Validation of these approximations requires pore-scale simulations. Our simulations suggest that the largest error stems from the localization, $\langle \langle c_1 \rangle^l \langle c_2 \rangle^l \rangle^l \approx \langle c_1 \rangle^l \langle c_2 \rangle^l$, of the product of macroscopic (averaged) concentrations $\langle c_i \rangle^l$ $(i = 1, 2)$ rather than from omission of the terms involving pore-scale fluctuations $\tilde{c}_i$. This suggests that a nonlocal (integro-differential) alternative of (22) and (23) might provide an accurate macroscopic approximation.
(4) Hybrid pore-scale/continuum-scale simulations [13,29] provide a more rigorous (and more computationally intensive) alternative. The scale-separation constraint (28) can facilitate such simulations by identifying the regions in a continuum computational domain where average (continuum-scale) concentration gradients exceed the given bound.

In follow-up studies, we will incorporate advection and dispersion into the analysis presented above, employ upscaling approaches other than the method of volume averaging to identify regions where continuum models break down, and develop hybrid algorithms which couple pore-scale simulations in these regions with continuum descriptions elsewhere in a computational domain.

Appendix A. Proofs of propositions

A.1. Proposition 3.1

A detailed derivation of the proof can be found in [32]. It is reproduced here for completeness in order to identify all the relevant constraints.

Applying the averaging theorem (10) to $\nabla_*^2 c_3$ twice, while accounting for the boundary condition (8), using the decomposition $c_3 = \langle c_3 \rangle^l + \tilde{c}_3$, and keeping the two leading terms in a Taylor expansion of the average concentration $\langle c_3 \rangle^l (\mathbf{x}^* + \mathbf{y}_l^*)$ under the volume integrals, one obtains [32, Eqs. 1.3-8]

$$\begin{aligned}\langle \nabla_*^2 c_3 \rangle = \nabla_* \cdot \Big(& \phi \nabla_* \langle c_3 \rangle^l - \nabla_* \langle \mathbf{y}_l^* \rangle \cdot \nabla_* \langle c_3 \rangle^l \\ & - \frac{1}{2} \nabla_* \langle \mathbf{y}_l^* \mathbf{y}_l^* \rangle : \nabla_* \nabla_* \langle c_3 \rangle^l \frac{1}{|\mathscr{V}|} \int_{A_{ls}} \tilde{c}_3 \mathbf{n} \, \mathrm{d}A \Big) \\ & - a_v D a_{ls} \frac{\langle c_3 \rangle_{ls} - 1}{l_l}, \end{aligned} \tag{A.1}$$

where

$$\langle c_3 \rangle_{ls} \equiv \frac{1}{|\mathscr{A}_{ls}|} \int_{\mathscr{A}_{ls}} c_3 \, \mathrm{d}A,$$

$\nabla_*\langle \mathbf{y}_l^* \rangle$ is a second order tensor and $\nabla_*\langle \mathbf{y}_l^*\mathbf{y}_l^* \rangle$ is a third-order tensor. The first constraint, $r_0 \gg l_l$, ensures that $\nabla_*\langle \mathbf{y}_l^* \rangle \cdot \nabla_*\langle c_3 \rangle^l$ is much smaller than $\phi\nabla_*\langle c_3 \rangle^l$ and, hence, can be neglected [32, p. 18]. The second constraint, $r_0^2 \ll L_\phi L_{c1}$, implies that $\nabla_*\langle \mathbf{y}_l^*\mathbf{y}_l^* \rangle : \nabla_*\nabla_*\langle c_3 \rangle^l$ is much smaller than $\phi\nabla_*\langle c_3 \rangle^l$ and can be neglected [32, p. 20]. With these approximations, (A.1) reduces to

$$\left\langle \nabla_*^2 c_3 \right\rangle = \nabla_* \cdot \left(\phi \nabla_* \langle c_3 \rangle^l + \frac{1}{|\mathscr{V}|} \int_{A_{ls}} \tilde{c}_3 \mathbf{n}\, \mathrm{d}A \right) - a_v Da_{ls} \frac{\langle c_3 \rangle_{ls} - 1}{l_l}. \tag{A.2}$$

To complete the proof, one has to show that $\langle c_3 \rangle_{ls}$ can be replaced with $\langle c_3 \rangle^l$. The third constraint, $l_l \ll L_c$, is required for the inequality $\langle c_3 \rangle^l \gg \tilde{c}_3$ to hold [32, p. 29, Eqs. 1.4-23], so that $\langle c_3 \rangle_{ls} \approx \langle \langle c_3 \rangle^l \rangle_{ls}$. The fourth, $r_0 \ll L_c$, and fifth, $r_0^2 \ll L_c L_{c1}$, constraints guarantee that $\langle \langle c_3 \rangle^l \rangle_{ls} \approx \langle c_3 \rangle^l$ [32, p. 20]. Substituting $\langle c_3 \rangle_{ls} = \langle c_3 \rangle^l$ into (A.2) leads to (14).

A.2. Proposition 3.2

Using the decomposition $c_i = \langle c_i \rangle^l + \tilde{c}_i$ $(i = 1, 2)$ in the average of the nonlinear term $\langle c_1 c_2 \rangle$ yields

$$\langle c_1 c_2 \rangle = \langle \langle c_1 \rangle^l \langle c_2 \rangle^l \rangle + \langle \tilde{c}_1 \langle c_2 \rangle^l \rangle + \langle \langle c_1 \rangle^l \tilde{c}_2 \rangle + \langle \tilde{c}_2 \tilde{c}_1 \rangle. \tag{A.3}$$

The constraint 3) of Proposition 3.1, $\epsilon \ll 1$, allows one to disregard the terms containing pore-scale fluctuations $\tilde{c}_i$ $(i = 1, 2)$ so that

$$\langle c_1 c_2 \rangle \approx \langle \langle c_1 \rangle^l \langle c_2 \rangle^l \rangle = \frac{1}{|\mathscr{V}|} \int_{V_l} \langle c_1 \rangle^l (\mathbf{x}^* + \mathbf{y}_l^*) \langle c_2 \rangle^l (\mathbf{x}^* + \mathbf{y}_l^*) \mathrm{d}^3 r. \tag{A.4}$$

Taylor expansions of the averaged concentrations around the centroid $\mathbf{x}^*$ leads to

$$\begin{aligned} \langle c_1 c_2 \rangle \approx{}& \phi \langle c_1 \rangle^l \langle c_2 \rangle^l + \langle c_1 \rangle^l \langle \mathbf{y}_l^* \rangle \cdot \nabla_* \langle c_2 \rangle^l + \frac{1}{2} \langle c_1 \rangle^l \langle \mathbf{y}_l^* \mathbf{y}_l^* \rangle \\ &: \nabla_* \nabla_* \langle c_2 \rangle^l + \langle c_2 \rangle^l \langle \mathbf{y}_l^* \rangle \cdot \nabla_* \langle c_1 \rangle^l + \frac{1}{2} \langle c_2 \rangle^l \langle \mathbf{y}_l^* \mathbf{y}_l^* \rangle \\ &: \nabla_* \nabla_* \langle c_1 \rangle^l + \nabla_* \langle c_1 \rangle^l \langle \mathbf{y}_l^* \mathbf{y}_l^* \rangle \nabla_* \langle c_2 \rangle^l + \cdots \end{aligned} \tag{A.5}$$

Since $\langle \mathbf{y}_l^* \rangle = \mathscr{O}(\phi r_0)$ [32, p. 31], the constraint 4) of Proposition 3.1, $r_0 \ll L_c$, gives the following estimate

$$\langle c_1 \rangle^l \langle \mathbf{y}_l^* \rangle \cdot \nabla_* \langle c_2 \rangle^l = \mathscr{O}\left(\frac{r_0}{L_c} \phi \langle c_1 \rangle^l \langle c_2 \rangle^l \right) \ll \langle c_1 \rangle^l \langle c_2 \rangle^l. \tag{A.6}$$

An analogous estimate holds for $\langle c_2 \rangle^l \langle \mathbf{y}_l^* \rangle \cdot \nabla_* \langle c_1 \rangle^l$. Since $\langle \mathbf{y}_l^* \mathbf{y}_l^* \rangle = \mathscr{O}(\phi r_0^2)$ [32, p. 19], the constraint 5) of Proposition 3.1, $r_0^2 \ll L_c L_{c1}$, leads to an estimate

$$\langle c_1 \rangle^l \langle \mathbf{y}_l^* \mathbf{y}_l^* \rangle : \nabla_* \nabla_* \langle c_2 \rangle^l = \frac{r_0^2}{L_c L_{c1}} \mathscr{O}\left(\phi \langle c_1 \rangle^l \langle c_2 \rangle^l \right) \ll \langle c_1 \rangle^l \langle c_2 \rangle^l. \tag{A.7}$$

An analogous estimate holds for $\langle c_2 \rangle^l \langle \mathbf{y}_l^* \mathbf{y}_l^* \rangle : \nabla_* \nabla_* \langle c_1 \rangle^l$. Finally, the constraint 4) of Proposition 3.1, $r_0^2 \ll L_c^2$, yields an estimate

$$\nabla_* \langle c_1 \rangle^l \langle \mathbf{y}_l^* \mathbf{y}_l^* \rangle \nabla_* \langle c_2 \rangle^l = \frac{r_0^2}{L_c^2} \mathscr{O}(\phi \langle c_1 \rangle^l \langle c_2 \rangle^l) \ll \langle c_1 \rangle^l \langle c_2 \rangle^l. \tag{A.8}$$

Substituting these estimates into (A.5) leads to the approximation (15).

A.3. Proposition 3.3

Given the approximations (14) and (15), the volume averaging of (6) yields

$$\begin{aligned} q \frac{\partial \langle c_3 \rangle^l}{\partial t} = \frac{q l_l^2}{Da} \left(\nabla_*^2 \langle c_3 \rangle^l + \frac{1}{\phi} \nabla_* \phi \cdot \nabla_* \langle c_3 \rangle^l + \frac{1}{\phi |\mathscr{V}|} \nabla_* \cdot \int_{A_{ls}} \tilde{c}_3 \mathbf{n}_{ls}\, \mathrm{d}A \right) \\ - \frac{q a_v l_l}{\phi} \frac{Da_{ls}}{Da} (\langle c_3 \rangle^l - 1) + \langle c_1 \rangle^l \langle c_2 \rangle^l - K \langle c_3 \rangle^l. \end{aligned} \tag{A.9}$$

The equation governing the dynamics of the concentration fluctuations $\tilde{c}_3$ is obtained by subtracting (A.9) from (6),

$$\begin{aligned} q \frac{\partial \tilde{c}_3}{\partial t} = \frac{q l_l^2}{Da} \left(\nabla_*^2 \tilde{c}_3 - \frac{1}{\phi} \nabla_* \phi \cdot \nabla_* \langle c_3 \rangle^l - \frac{1}{\phi |\mathscr{V}|} \nabla_* \cdot \int_{A_{ls}} \tilde{c}_3 \mathbf{n}_{ls}\, \mathrm{d}A \right) \\ + \frac{q a_v l_l}{\phi} \frac{Da_{ls}}{Da} (\langle c_3 \rangle^l - 1) + c_1 c_2 - \langle c_1 \rangle^l \langle c_2 \rangle^l - K \tilde{c}_3. \end{aligned} \tag{A.10}$$

The constraint 1) of Proposition 3.3, $a_v \approx l_l^{-1}$, implies that the integral term in (A.10) is much smaller than $\nabla_*^2 \tilde{c}_3$ and, hence, can be neglected [32, p. 26]. If $t \gg Da$, the constraint 2) of Proposition 3.3, the closure problem can be considered quasi-steady, i.e., the time derivative in (A.10) can be dropped. The constraint 3) of Proposition 3.3, $l_l \ll L_\phi$, ensures that $\phi^{-1} \nabla_* \phi \cdot \nabla_* \langle c_3 \rangle^l$ can be neglected [32, p. 27]. Combining these approximations with the decomposition $c_i = \langle c_i \rangle^l + \tilde{c}_i$ $(i = 1, 2)$ of the term $c_1 c_2$ in (A.10) yields the equation for fluctuations (16). A similar procedure leads to the boundary condition (17).

A.4. Proposition 3.4

Further progress requires one to assume that a porous medium is spatially periodic [4,32]. This allows one to solve for $\tilde{c}$ in some representative region and then use this solution to construct a closure. Since boundary conditions on the surface of a computational domain have negligible influence on $\tilde{c}$-field almost everywhere [18], one can impose a periodic condition at the boundary of the unit cell, $\tilde{c}(\mathbf{r}^* + \mathbf{l}_i^*) = \tilde{c}(\mathbf{r}^*)$, where $\mathbf{l}_i^*$ $(i = 1, 2, 3)$ represent the three non-unique lattice vectors describing a spatially periodic porous medium. It is important to recognize that this periodic boundary condition is consistent with the equations for fluctuations only if the geometry is periodic and source terms are either constant or spatially periodic inside the representative volume.

Expanding $\langle c_3 \rangle^l$ and $\nabla_* \langle c_3 \rangle^l$ in (16) and (17) into Taylor series around the centroid $\mathbf{x}^*$ and invoking the constraint 4) of Proposition 3.1 to neglect the higher-order terms, one obtains a local formulation for the $\tilde{c}_3$-field [32, p. 32]. In this formulation, reactive sources (the terms proportional to $\langle c_i \rangle^l$) and diffusive sources (the terms proportional to $\nabla_* \langle c_i \rangle^l$) are evaluated at the centroid $\mathbf{x}^*$ and, hence, are treated as constant and spatially periodic, respectively [32, p. 32]. This ensures that the periodic boundary conditions $\tilde{c}(\mathbf{r}^* + \mathbf{l}_i^*) = \tilde{c}(\mathbf{r}^*)$ are consistent with (16) and (17).

A.5. Proposition 3.5

Let $c_4 \equiv c_3 - 1$. Hence, $\langle c_3 \rangle^l - 1 = \langle c_4 \rangle^l$ and $\tilde{c}_3 = \tilde{c}_4$. An equation and a boundary condition for deviation $\tilde{c}_4$ can be obtained respectively from (16) and (17) through the previous substitutions. An order-of-magnitude analysis of boundary condition for $\tilde{c}_4$ leads to estimates

$$\tilde{c}_4 = \mathscr{O}\left(\frac{\epsilon + Da_{ls}}{1 + Da_{ls}} \langle c_4 \rangle^l \right) \Rightarrow \tilde{c}_4 = \mathscr{O}(\epsilon \langle c_4 \rangle^l). \tag{A.11}$$

The second estimate in (A.11) stems from the constraint 3) of Proposition 3.1, $\epsilon \ll 1$, and the constraint 1) of Proposition 3.5, $Da_{ls} \ll \epsilon$. The estimate (A.11) allows one to simplify the boundary condition for $\tilde{c}_4$ and consequently to approximate the boundary condition (17) with

$$-\mathbf{n} \cdot \nabla_* \tilde{c}_3 = \mathbf{n} \cdot \nabla_* \langle c_3 \rangle^l + Da_{ls} \frac{\langle c_3 \rangle^l - 1}{l_l} \quad \text{on } \mathscr{A}_{ls}. \tag{A.12}$$

The estimate (A.11) also leads to the following order-of-magnitude estimates of the terms in the equation for $\tilde{c}_4$: $q l_l^2 \nabla_*^2 \tilde{c}_4 / Da = \mathscr{O}(q\epsilon \langle c_4 \rangle^l / Da)$, $q a_v l_l Da_{ls} \langle c_4 \rangle^l / \phi Da = \mathscr{O}(q Da_{ls} \langle c_4 \rangle^l / Da)$, $K\tilde{c}_4 = \mathscr{O}(\epsilon K \langle c_4 \rangle^l)$, $\langle c_i \rangle^l \tilde{c}_j = \mathscr{O}(\epsilon \langle c_i \rangle^l \langle c_j \rangle^l)$ for $i,j = \{1,2\}$ such that $i \neq j$, and

$\tilde{c}_1\tilde{c}_2 = \mathcal{O}(\epsilon^2\langle c_1\rangle^l\langle c_2\rangle^l)$. An order-of magnitude relation between $\langle c_4\rangle^l$ and $\langle c_1\rangle^l$ (or $\langle c_2\rangle^l$) is needed in order to compare the terms containing perturbations $\tilde{c}_1$ and $\tilde{c}_2$ with those containing $\tilde{c}_4$ and $\langle c_4\rangle^l$. It is obtained from equations for $\tilde{c}_1$ (or $\tilde{c}_2$) by recognizing that $-l_l^2\nabla_*^2\tilde{c}_1/Da = ql_l^2\nabla_*^2\tilde{c}_4/Da + qa_v l_l Da_{ls}\langle c_4\rangle^l/\phi Da$, which leads to estimates

$$\langle c_4\rangle^l = \mathcal{O}\left(\frac{\epsilon}{\epsilon + Da_{ls}}\frac{\langle c_1\rangle^l}{q}\right) \Rightarrow \langle c_4\rangle^l = \mathcal{O}\left(\frac{\langle c_1\rangle^l}{q}\right). \tag{A.13}$$

The estimate (A.13) combined with the constraint 2) of Proposition 3.5 allows one to neglect the terms containing deviation $\tilde{c}_1$ and $\tilde{c}_2$ (i.e., $\tilde{c}_1\tilde{c}_2$ and $\langle c_i\rangle^l\tilde{c}_j$ for $i,j = \{1,2\}$ such that $i \neq j$) relative to the diffusion term $ql_l^2\nabla_*^2\tilde{c}_4/Da$. For example, the order of magnitude of the ratio between $ql_l^2\nabla_*^2\tilde{c}_4/Da$ and $\langle c_1\rangle^l\tilde{c}_2$ is $\mathcal{O}(Da\langle c_2\rangle^l)$ for $\langle c_1\rangle^l \neq 0$. Since $0 \leqslant \langle c_2\rangle^l \leqslant 1$, this yields $\langle c_1\rangle^l\tilde{c}_2 \ll ql_l^2\nabla_*^2\tilde{c}_4/Da$ if $Da \ll 1$. Neglecting the fluctuation terms in the equation for $\tilde{c}_4$ allows one to approximate (16) as

$$\nabla_*^2\tilde{c}_3 - \frac{k_3}{\mathscr{D}}\tilde{c}_3 = -\frac{a_v Da_{ls}}{\phi l_l}(\langle c_3\rangle^l - 1) \quad \text{in } V_l. \tag{A.14}$$

In the spirit of [32], we represent a solution of (A.12) and (A.14) as

$$\tilde{c}_3 = \mathbf{b}^*\cdot\nabla_*\langle c_3\rangle^l + s\langle c_3\rangle^l + \psi, \tag{A.15}$$

where $\mathbf{b}^*, s$ and ψ are undetermined functions called closure variables. They are specified as solutions of the boundary-value problems (19)–(21), which are obtained by substituting (A.15) into (A.14).

Constraint 2 of Proposition 3.5 is required for similar analyses of equations for c_1 and c_2.

A.6. Miscellaneous

Derivation of (22) and (23). Substitution of (A.15) into (A.9) gives

$$q\frac{\partial\langle c_3\rangle^l}{\partial t} = \frac{ql_l^2}{\phi Da}\nabla_*\cdot[\phi(\mathbf{D}_{\text{eff}}\cdot\nabla_*\langle c_3\rangle^l + \mathbf{u}\langle c_3\rangle^l + \mathbf{p})] - \frac{qa_v l_l}{\phi}\frac{Da_{ls}}{Da}[\langle c_3\rangle^l - 1] + \langle c_1\rangle^l\langle c_2\rangle^l - K\langle c_3\rangle^l \tag{A.16}$$

where $\mathbf{D}_{\text{eff}}$ is given by (24) and $\mathbf{u}$ and $\mathbf{p}$ are defined as

$$\mathbf{u} = \frac{1}{|V_l|}\int_{A_{ls}} s\mathbf{n}_{ls}\,dA, \quad \mathbf{p} = \frac{1}{|V_l|}\int_{A_{ls}}\psi\mathbf{n}_{ls}\,dA. \tag{A.17}$$

The constraint 1 of Proposition 3.3, $a_v \approx l_l^{-1}$, and Eq. (20), that provides an estimate for s, imply that $ql_l^2\nabla_*\cdot(\phi\mathbf{u}\langle c_3\rangle^l)/\phi Da$ is much smaller than $qa_v l_l Da_{ls}\langle c_3\rangle^l/\phi Da$ and, thus, can be neglected [32, p. 36]. Similar results can be obtained for $ql_l^2\nabla_*\cdot(\phi\mathbf{p})/\phi Da$ that can be neglected relative to $qa_v l_l Da_{ls}/\phi Da$. With these approximations (A.16) reduces to (23), wherein the space coordinates are scaled with a typical macroscopic length, e.g., L_c.

A similar procedure leads to (22).

Analysis of Ochoa-Tapia et al. [17]. The derivation of macroscopic Eqs. (22) and (23) is tantamount to a closure for $\langle c_1c_2\rangle$ in which all terms containing concentration fluctuations, i.e., $\tilde{c}_1\tilde{c}_2$ and $\tilde{c}_k\langle c_j\rangle^l$ $(k,j = \{1,2\}$ such that $k \neq j)$, are neglected. It requires the set of constraints specified in Propositions 3.1–3.5. Ochoa-Tapia et al. [17] neglect $\tilde{c}_1\tilde{c}_2$ while retaining $\tilde{c}_k\langle c_j\rangle^l$ $(k,j = \{1,2\}$ such that $k \neq j)$. This leads to a closure for $\langle c_1c_2\rangle$ where one of these constraints, $Da \ll 1$, needs to be replaced with $1 \ll Da \ll 1/\epsilon$. The closure results in a system of equations for pore-scale fluctuations $A_{ij}\tilde{c}_j = b_i$—where $A_{11} = (l_l^2/Da)\nabla_*^2 - \langle c_2\rangle^l$, $A_{22} = (l_l^2/Da)\nabla_*^2 - \langle c_1\rangle^l$, $A_{33} = (ql_l^2/Da)\nabla_*^2 - K$, $A_{12} = -\langle c_1\rangle^l$, $A_{21} = -\langle c_2\rangle^l$, $A_{31} = \langle c_2\rangle^l$, $A_{32} = \langle c_1\rangle^l$, $b_3 = -(qa_v l_l Da_{ls}/\phi Da)(\langle c_3\rangle^l - 1)$, $A_{13} = A_{23} = K$ and $b_1 = b_2 = 0$—that must be solved *simultaneously* with a macroscopic problem (see Fig. 1).

References

[1] Acharya RC, der Zee SEATMV, Leijnse A. Transport modeling of nonlinearly adsorbing solutes in physically heterogeneous pore networks. Water Resour Res 2005;41:W02020.

[2] Adler PM. Porous media: geometry and transports. Heinemann: Butterworth; 1992.

[3] Auriault JL, Adler PM. Taylor dispersion in porous media: analysis by multiple scale expansions. Adv Water Resour 1995;18(4):217–26.

[4] Brenner H. Transport processes in porous media. McGraw-Hill; 1987.

[5] Duijn CJV, Pop IS. Crystal dissolution and precipitation in porous media: pore-scale analysis. J Reine Angew Math 2004;577:171–211.

[6] Gray WG, Miller CT. Thermodynamically constrained averaging theory approach for modeling flow and transport phenomena in porous medium systems: 1. Motivation and overview. Adv Water Resour 2005;28(2):161–80.

[7] Jacobson RL, Langmuir D. Dissociation constant of calcite and $CaHCO_3^+$ from 0 to 50 c. Geochim Cosmochim Acta 1974;38:301–18.

[8] Jiang Z, Ebner C. Simulation study of reaction fronts. Phys Rev A 1990;42:7483–6.

[9] Kechagia PE, Tsimpanogiannis IN, Yortsos YC, Lichtner PC. On the upscaling of reaction-transport processes in porous media with fast or finite kinetics. Chem Eng Sci 2002;57(13):2565–77.

[10] Knabner P, Duijn CJV, Hengst S. An analysis of crystal dissolution fronts in flows through porous media. Part 1: Compatible boundary conditions. Adv Water Resour 1995;18(3):171–85.

[11] Knutson C, Valocchi A, Werth C. Comparison of continuum and pore-scale models of nutrient biodegradation under transverse mixing conditions. Adv Water Resour 2007;30(6–7):1421–31.

[12] Kundu PK, Cohen IM. Fluid mechanics. 4th ed. San Diego: Elsevier; 2008.

[13] Leemput PV, Vandekerckhove C, Vanroose W, Roose D. Accuracy of hybrid lattice Boltzmann/finite difference schemes for reaction–diffusion systems. Multiscale Model Simul 2007;6(3):838–57.

[14] Maloy KJ, Feder J, Boger F, Jossang T. Fractal structure of hydrodynamic dispersion in porous media. Phys Rev Lett 1998;61(82):2925.

[15] Neuman SP, Tartakovsky DM. Perspective on theories of anomalous transport in heterogeneous media. Adv Water Resour 2008. doi:10.1016/j.advwatres.2008.08.005.

[16] Nitsche LC, Brenner H. Eulerian kinematics of flow through spatially periodic models of porous media. Arch Ration Mech Anal 1989;107(3):225–92.

[17] Ochoa-Tapia JA, Stroeve P, Whitaker S. Facilitated transport in porous media. Chem Eng Sci 1991;46:477–96.

[18] Pratt M. On the boundary conditions at the macroscopic level. Transport Porous Media 1989;4:259–80.

[19] Quintard M, Whitaker S. Transport in ordered and disordered porous media II: Generalized volume averaging. Transport Porous Media 1994;14:179–206.

[20] Reddy MM, Plummer LN, Busenberg E. Crystal growth of calcite from calcium bicarbonate solutions at constant p_{CO_2} and 25 c: a test for calcite dissolution model. Geochim Cosmochim Acta 1981;45:1281–9.

[21] Sahimi M. Flow phenomena in rocks: from continuum models to fractals percolation, cellular, automata, and simulated annealing. Rev Mod Phys 1993;65(4):1393–534.

[22] Shapiro M, Brenner H. Taylor dispersion of chemically reactive species: irreversible first-order reactions in bulk and on boundaries. Chem Eng Sci 1986;41(6):1417–33.

[23] Shapiro M, Brenner M. Dispersion of a chemically reactive solute in a spatially periodic model of a porous medium. Chem Eng Sci 1988;43(3):551–71.

[24] Shapiro M, Fedou R, Thovert J, Adler PM. Coupled transport and dispersion of multicomponent reactive solutes in rectilinear flows. Chem Eng Sci 1996;51(22):5017–41.

[25] Steefel CI, DePaolo DJ, Lichtner PC. Reactive transport modeling: an essential tool and a new research approach for the Earth sciences. Earth Planet Sci Lett 2005;240:539–58.

[26] Tartakovsky AM, Meakin P, Scheibe TD, West RME. Simulation of reactive transport and precipitation with smoothed particle hydrodynamics. J Comput Phys 2007;222:654–72.

[27] Tartakovsky AM, Redden G, Lichtner PC, Scheibe TD, Meakin P. Mixing-induced precipitation: experimental study and multi-scale numerical analysis. Water Resour Res 2008;44:W06S04. doi:10.1029/2006WR005725.

[28] Tartakovsky AM, Tartakovsky DM, Meakin P. Stochastic Langevin model for flow and transport in porous media. Phys Rev Lett 2008;101:044502.

[29] Tartakovsky AM, Tartakovsky DM, Scheibe TD, Meakin P. Hybrid simulations of reaction–diffusion systems in porous media. SIAM J Sci Comput 2007;30(6):2799–816.

[30] van Noorden TL, Pop IS. A Stefan problem modelling crystal dissolution and precipitation. IMA J Appl Math 2008;73(2):393–411.

[31] Whitaker S. Flow in porous media I: a theoretical derivation of Darcy's law. Transport Porous Media 1986;1:3–25.

[32] Whitaker S. The method of volume averaging. Netherlands: Kluwer Academic Publishers; 1999.
[33] Wood BD, Ford RM. Biological processes in porous media: from the pore scale to the field. Adv Water Resour 2007;30(6–7):1387–91.
[34] Wood BD, Radakovich K, Golfier F. Effective reaction at a fluid–solid interface: applications to biotransformation in porous media. Adv Water Resour 2007;30(6–7):1630–47.